2018

Validation of a Charge-Sensitive Vapor-Injected Compression Cycle Model with Economization

Ammar M. Bahman
Ray W. Herrick Laboratories, Purdue University, United States of America, abahman@purdue.edu

Davide Ziviani
School of Mechanical Engineering, Ray W. Herrick Laboratories, Purdue University, dziviani@purdue.edu

Eckhard A. Groll
Purdue University - Main Campus, groll@purdue.edu

Validation of a Charge-Sensitive Vapor-Injected Compression Cycle Model with Economization

Ammar M. BAHMAN[1,2,*], Davide ZIVIANI[2], Eckhard A. GROLL[2]

[1]Kuwait University, College of Engineering and Petroleum, Mechanical Engineering Department, Kuwait City, Kuwait
a.bahman@ku.edu.kw

[2]Purdue University, School of Mechanical Engineering, Ray W. Herrick Laboratories, West Lafayette, Indiana, USA
abahman@purdue.edu, dziviani@purdue.edu, groll@purdue.edu

* Corresponding Author

ABSTRACT

In recent years, research on economized vapor injected (EVI) compression systems showed potential improvements to both cooling capacity and coefficient of performance (COP). In addition, the operating range of compressors can be extended by reducing the discharge temperature. However, the optimum operation of such systems is directly related to the amount of refrigerant charge, which often is not optimized. Therefore, an accurate charge estimation methodology is required to further improve the operation of EVI compression systems. In this paper, a detailed cycle model has been developed for the EVI compression system. The model aims to predict the performance of EVI systems by imposing the amount of required refrigerant charge as an input. In the cycle model, the EVI compressor was mapped based on the correlation of Tello-Oquendo et al. (2017), whereas evaporator, condenser and economizer heat exchanger models were constructed based on the available ACHP models (Bell, 2015). With respect to charge inventory, the two-point regression model from Shen et al. (2009) was used to account for inaccurate estimation of refrigerant volumes, ambiguity in slip flow model, and solubility of refrigerant in the lubricating oil. The cycle model has been validated with experimental performance data taken with a 5-ton Environmental Control Unit (ECU) that utilizes EVI technology. The developed cycle model showed very good agreement with the data with a MAE in COP of less than 5%. Furthermore, the estimated charge inventory has been compared to the one-point regression model. Results showed that the former method allowed to predict the charge inventory with an MAE of less than 0.2%.

1. INTRODUCTION

Vapor injection systems for heating, cooling, and refrigeration (HVAC&R) applications are characterized by higher performance with respect to the conventional vapor compression systems. In particular, an economized vapor injection (EVI) compression system aims to cool the refrigerant during the compression process by injecting the refrigerant vapor at an intermediate stage into the compressor, as shown in Figure 1a. Therefore, the compressor discharge temperature is reduced, and the compressor operating range is extended to a larger temperature lift. Research on EVI systems showed potential improvements to both cooling capacity and system COP (Bertsch and Groll, 2008; Tello-Oquendo et al., 2016; Cho et al., 2016). In recent studies, researchers developed numerical EVI system models to evaluate the performance of the systems (Wang et al., 2009; Lee et al., 2015; Sun et al., 2018), which they utilized the models for control purposes, and they showed the importance of charge inventory. Although charge inventory has a strong influence on the overall system performance, the application of a charge-sensitive EVI system model is still lacking in the literature.

The purpose of this study is to develop a detailed EVI cycle model and to estimate the amount of required refrigerant charge needed for EVI system to operate effectively. A 5-ton Environmental Control Unit (ECU) was tested at high ambient conditions to validate the model developed herein. The refrigerant charge predictions are estimated with one- and two-point regression model and compared with the experimental data.

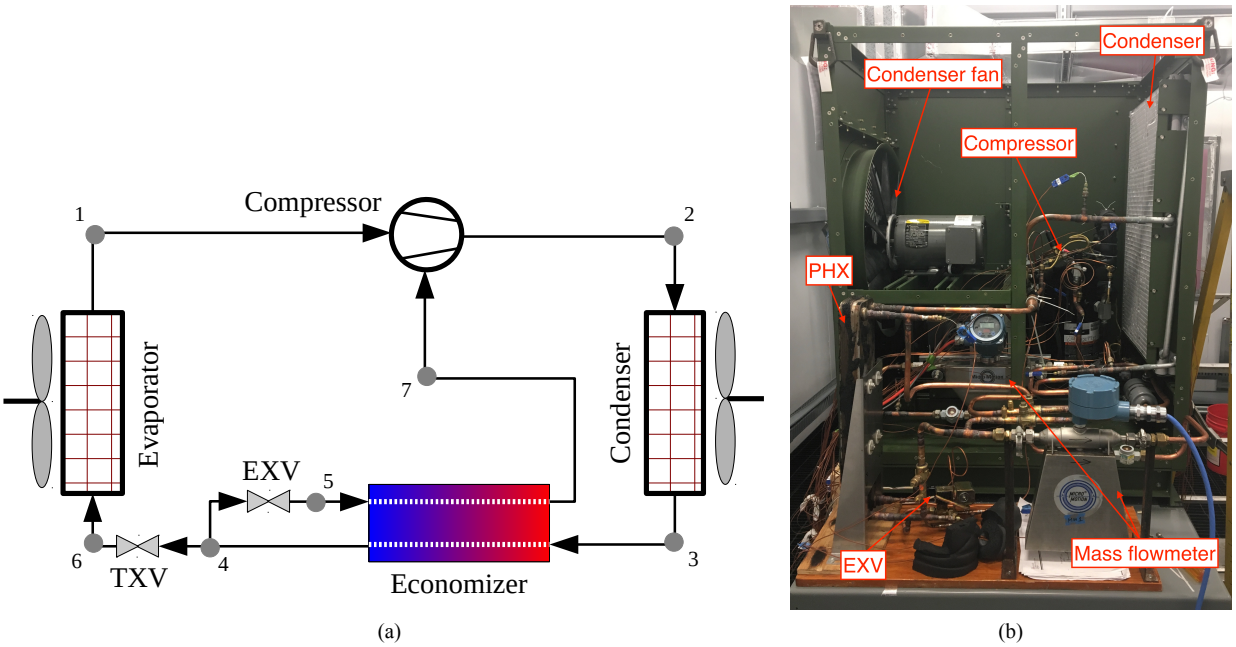

Figure 1: (a) Economized vapor injection (EVI) compression system diagram.; (b) view of the Environmental Control Unit (ECU) retrofitted with EVI system.

2. MODEL DESCRIPTION

A packaged ECU for military applications was considered to conduct numerical and experimental studies. The schematic of the system is shown in Figure 1b, and the components are simulated in an object-oriented fashion by using the programming language Python (2016). The thermo-physical properties of the working fluid (R-407C) were obtained from Bell et al. (2014). In the model, both evaporator and condenser fans were modeled by using experimental average values for steady-state operation. The average airflow rate and power consumption for the evaporator fan were equal to 0.8023 m^3/s and 0.77 kW, respectively. The airflow across the condenser fan was equal to 1.746 and 1.18 m^3/s for high and low operation modes, corresponding to average measured power consumption of 1.032 kW and 0.396 kW, respectively. Note that the linesets (*i.e.,* suction line, discharge line and liquid line) were excluded in the model due to their short lengths. However, the volume of the filter drier, sight glasses, and mass flow meters in the liquid line were considered for the purposed of charge calculations. This proposed EVI model includes: compressor, evaporator, condenser, economizer, expansion valves, and charge models, each of which is explained in the following sections.

2.1 Compressor Model

The single-port vapor-injected compressor model described by Tello-Oquendo et al. (2017) was used where the compressor map coefficients were fitted using the experimental data from Lumpkin et al. (2018) to calculate the suction mass flow rate, the injection mass flow ratio, and the power consumption. To accurately estimate the refrigerant charge dissolved in the compressor's lubricant, Harms (2002) charge solubility model for the mixture of R-407C and POE32 oil was used. The amount of refrigerant charge dissolved in oil is determined by

$$m_{charge} = \rho_{shell} V_{oil} \left(\frac{\zeta}{1-\zeta} \right) \tag{1}$$

where V_{oil} is the initial oil volume (64 oz.), and the refrigerant solubility fraction is given by

$$\zeta = \frac{P}{990 + 91.9T + 0.633T^2} \tag{2}$$

2.2 Heat Exchangers Model

The condenser and evaporator heat exchanger models from the ACHP model (Bell, 2015) were modified to be used in this work. The condenser model was constructed using a moving boundary method, which divides the condenser according to the phases of refrigerant flow. Each section of the condenser model was simulated using the ε-NTU method as separate crossflow multi-louvered micro-channel heat exchangers (Lee, 2010), assuming constant refrigerant pressure equal to the inlet pressure. To accurately estimate the refrigerant charge in the two-phase region, Zivi (1964) slip flow model was used in the condenser model. The correlations used to estimate the heat transfer coefficients and friction factors in the micro-channel condenser model are summarized in Table 1, while the geometrical parameters used are listed in Table 2. To accurately estimate the behavior of the heat transfer from the air to the refrigerant side

Table 1: Heat transfer and pressure drop correlations in micro-channel condenser model.

		Single-phase	Two-phase
Refrigerant-side	Heat transfer	Gnielinski (1976)	Kim and Mudawar (2013)
	Pressure drop	Churchill (1977)	Kim and Mudawar (2012)
Air-side	Heat transfer	Kim and Bullard (2002)	
	Friction factor	Chang et al. (2000)	

Table 2: Geometrical parameters in the micro-channel condenser model.

Number of tubes per slab	52
Number of passes per slab	2
Number of slabs	2
Number of ports (channels)	11
Length of tubes [mm]	540
Width of tubes [mm]	25.4
Height of tubes (major diameter) [mm]	1.8288
Wall thickness of tubes [mm]	0.381
Wall thickness of ports [mm]	0.4064
Aspect ratio of ports	1.7675
Fins per inch	14
Fin height [mm]	12.3952
Fin thickness [mm]	0.1143
Louver height [mm]	25.4
Louver pitch [mm]	1.12
Louver angle [degree]	25
Conductivity of fins [W/m-K]	117

of the evaporator, the partially-wet and partially-dry method (Braun, 1988) is utilized in predicting the air side sensible and latent heat transfer when the surface temperature of the coil falls below the dew-point of air at the inlet of the evaporator.

The evaporator model was solved by separating the heat exchanger into two sections. The section with surface temperatures higher than the dew-point was solved by a completely dry analysis, while the other section was solved assuming a completely wet analysis. Likewise as in the condenser, Zivi (1964) slip flow model was used in the evaporator model to estimate the refrigerant charge in the two-phase region. The correlations used to solve the heat transfer coefficients and friction factors in the evaporator model are presented in Table 3, while the geometrical parameters shown in Table 4 are used.

2.3 Economizer Model

The plate heat exchanger (PHX) model proposed by (Bell et al., 2015) was used. The model was constructed with robust steady-state, counter-flow, moving-boundary model. The model accounts for any phase condition for both hot and cold streams. In addition, the model efficiently utilizes internal and external pinching points, allowing for the possibility of mixed phase combinations in both refrigerant streams. For example, in the most general case of the counter-flow

Table 3: Heat transfer and pressure drop correlations in evaporator model.

		Single-phase	Two-phase
Refrigerant-side	Heat transfer	Gnielinski (1976)	Shah (1976)
	Pressure drop	Churchill (1977)	Lockhart and Martinelli (1949)
Air-side	Heat transfer	Wang et al. (1998)	
	Fin efficiency	Schmidt (1945) modified by Hong and Webb (1996)	

Table 4: Geometrical parameters in the evaporator model.

Number of tubes per bank	18
Number of banks	4
Number of circuits	6
Length of tubes [mm]	631.825
Outer diameter of tubes [mm]	12.7
Inner diameter of tubes [mm]	11.7348
Longitudinal distance of tubes [mm]	27.4828
Transverse distance of tubes [mm]	131.75
Fins per inch	12
Fin waviness [mm]	0.79375
Half-wavelength of fin wave [mm]	6.35
Fin thickness [mm]	0.1905
Conductivity of fins [W/m-K]	237

Table 5: Geometrical parameters in the PHX economizer model.

Number of plates	10
Length of plates [mm]	457.2
Width of plates [mm]	73.025
Thickness of plates [mm]	0.3
Wavelength of plates [mm]	6.26
Amplitude of corrugation [mm]	1
Chevron angle [degree]	65
Conductivity of plates [W/m-K]	15

moving-boundary PHX model, both streams enter with single-phase states, undergo complete phase change, and exit with single-phase states. This results in five separate zones in which each zone is defined by the phase boundary of each one of the streams. Note that the economizer is assumed to be insulated and exhibits no heat loss with the surroundings. In the PHX model, Zivi (1964) slip flow model was used to calculate the refrigerant charge in the two-phase region. The geometrical parameters of the PHX are listed in Table 5. Whereas, the heat transfer coefficients and friction factors correlations of the economizer model are summarized in Table 6.

Table 6: Heat transfer and pressure drop correlations in economizer model.

		Single-phase	Two-phase
Hot-side	Heat transfer	Martin (2010)	Longo et al. (2004); Longo (2010,0)
	Pressure drop		Lockhart and Martinelli (1949)
Cold-side	Heat transfer	Martin (2010)	Cooper (1984)
	Pressure drop		Lockhart and Martinelli (1949) modified by Claesson (2004)

2.4 Expansion Valves Model

In this work, the expansion process modeling approach was implemented using adjustable throat-area devices. The adjustable throat-area expansion devices include thermostatic expansion valves (TXV) and electronic expansion valve (EXV). Li and Braun (2008) method was used to model adjustable throat-area expansion valves by using experimental rating data. Both linear- and non-linear models were implemented for the TXV and EXV devices, respectively. The linear and non-linear expansion model are expressed in Equations 3 and 4, respectively. Whereas the coefficients of the model were tuned using manufacturer's data and summarized in Table 7.

$$\dot{m}_{TXV} = C\left(T_{sh} - T_{sh,static}\right)\sqrt{\rho_{up}\left(P_{up} - P_{down}\right)} \tag{3}$$

$$\dot{m}_{EXV} = C\left[2\left(\frac{T_{sh} - T_{sh,static}}{T_{sh,max}}\right) - \left(\frac{T_{sh} - T_{sh,static}}{T_{sh,max}}\right)^2\right]\sqrt{\rho_{up}\left(P_{up} - P_{down}\right)} \tag{4}$$

Table 7: Expansion valve model geometrical parameters and mapped coefficients.

	TXV	EXV
D [mm]	12.7	6.35
$T_{sh,static}$ [K]	4	2
$T_{sh,max}$ [K]	–	10
C	6.3×10^{-7}	6.328×10^{-7}

Table 8: Charge model tunning coefficients.

C [kg]	3.1
K	−0.273
w_{ref}	0.184

2.5 Charge Model

Due to the inaccurate estimation of the system volumes, ambiguous flow patterns under two-phase flow conditions, etc., a single-point and a two-point charge tuning procedures were implemented based on the methodology proposed and validated by Shen et al. (2009). In particular, the total refrigerant charge of the system is given by the sum of the mass calculated by the cycle model and a contribution fitted onto the experimental data which can be expressed as

$$m_{charge} = m_{pred} + \Delta m_{liq} \tag{5}$$

with

$$\Delta m_{liq} = C + K\left(w_{liq,pred} - w_{ref}\right) \tag{6}$$

where C, K, and w_{ref} are the coefficients to be determined through only two experimental data points to calibrate the model. The tunning coefficients are listed in Table 8. Note that for the one-point regression model, Equation (6) results with the coefficient C only.

2.6 Pre-Conditioner Model

In order to obtain good initial guesses and reduce computational time for the main cycle solver, a pre-conditioner model from Bell (2015) was modified to estimate values for refrigerant dew-point temperatures in evaporator, condenser, and economizer (cold-side). The pre-conditioner model emulates the main cycle to be solved with simplified models for condenser, evaporator and economizer, as shown in Figure 2a. The independent variables (*i.e.,* T_{evap}, T_{cond}, and $T_{dew,inj}$) are iterated to minimize the residual vector (Equation 7) by means of *fsolve* function (Moré et al., 1980) until convergence. Note that the superheat of the suction and injection lines (*i.e.,* $T_{sh,suc}$ and $T_{sh,inj}$) are deterministically evaluated in the main cycle. However, in the pre-conditioner model targeted values were used as inputs to ensure continuity.

$$\vec{\Delta} = \begin{bmatrix} \dot{W}_{comp} + \dot{Q}_{evap} - \dot{Q}_{cond} - \dot{Q}_{econ,h} \\ \dot{Q}_{cond,a} - \dot{Q}_{cond,r} \\ \dot{Q}_{econ,h} - \dot{Q}_{econ,c} \end{bmatrix} \tag{7}$$

2.7 System-Level Model

The flow chart in Figure 2b shows the algorithm used in the system-level solver. The components in the system-level model were simulated consecutively as shown in Figure 2b. Due to the fact that the economizer model needs the information of the inlets on both hot and cold sides, the inlet quality of the cold-side is iterated to ensure the energy balance on the economizer, as show in Equation 8. Equation 8 is driven to zero by means of Brent (1973) method.

$$\dot{m}_{tot} h_{cond,out} - \dot{m}_{suc} h_{econ,h,out} - \dot{m}_{inj} h_{econ,c,out} = 0 \tag{8}$$

The independent variables (*i.e.,* T_{evap}, T_{cond}, $T_{dew,inj}$, $T_{sh,suc}$, and $T_{sh,inj}$) are iterated by means of Broyden (1965) method to drive the residual vector to zero, as shown in Equation 9.

$$\vec{\Delta} = \begin{bmatrix} m_{charge} - m_{charge,target} \\ h_{econ,c,out} - h_{comp,inj} \\ h_{evap,out} - h_{comp,in} \\ \dot{m}_{suc} - \dot{m}_{TXV} \\ \dot{m}_{inj} - \dot{m}_{EXV} \end{bmatrix} \tag{9}$$

The model checks for the pressure drop residual after the residual vector converges, as expressed by Equation 10. The pressure drops in the high-, low- and intermediate-lineset are considered after the cycle iteration completed to avoid numerical difficulties. Hence, new effective saturation temperatures (*i.e.,* T^*_{cond}, T^*_{evap}, and $T^*_{dew,inj}$) are calculated, and iterated in the cycle model until the updated effective pressure drop (*i.e.,* P^*_{high}, P^*_{low}, and P^*_{int}) are equal to the pressure drop terms calculated from the converged cycle model (*i.e.,* P_{high}, P_{low}, and P_{int}).

$$\vec{\Delta P} = \begin{bmatrix} P^*_{high} - P_{high} \\ P^*_{low} - P_{low} \\ P^*_{int} - P_{int} \end{bmatrix} \tag{10}$$

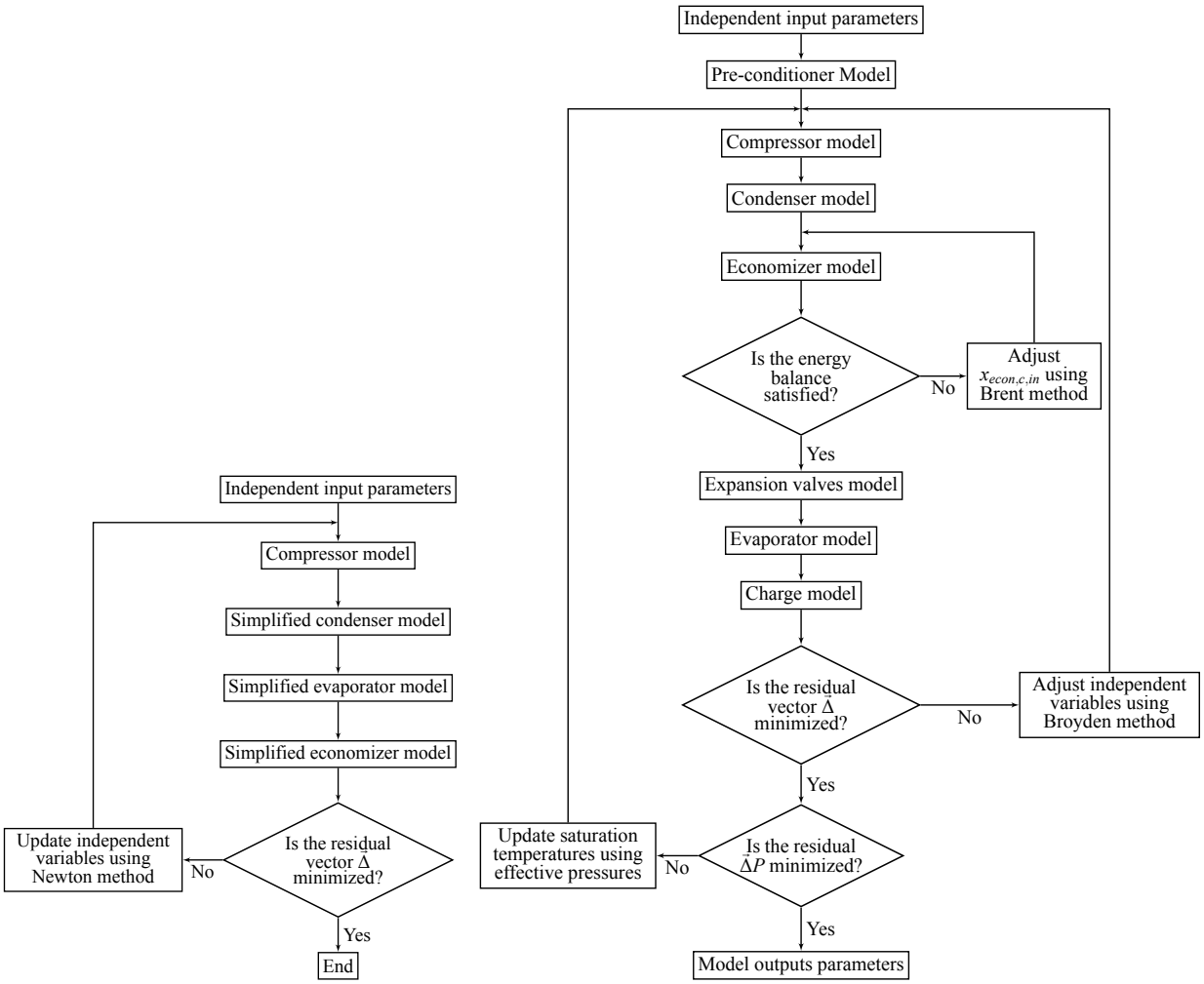

(a) Pre-conditioner solver algorithm (b) Cycle solver algorithm

Figure 2: Flowcharts of pre-conditioner model and EVI cycle solvers.

3. RESULTS AND DISCUSSION

3.1 Experimental Methodology

An Environmental Control Unit (ECU) that has a rated cooling capacity of 17.6 kW (60,000 Btu/hr) was retrofitted with EVI system and tested under the same operating conditions in side-by-side psychrometric chambers at the Herrick

Laboratories. The test conditions are reported in Table 9. Note that Test Conditions 4/A, B and C are compliant with ASHRAE Standard 210/240 (Standard, 2008), while Test Conditions 1 and 2 represent extreme ambient temperatures. The ECU was charged under the same operating condition of Test 4/A for testing the EVI system with superheated-injection ($T_{sh,inj}$ = 7°C). The unit was charged with 5.01 kg (11.05 lb) of refrigerant R-407C to maintain injection superheat of 7°C and ensure consistent subcooling of 5°C in the liquid line.

Table 9: Rating testing conditions of ECU experimental testing.

Test No.	Outdoor condition				Indoor condition				Description
	Dry-bulb		Wet-bulb		Dry-bulb		Wet-bulb		
	°C	°F	°C	°F	°C	°F	°C	°F	
1	51.7	125	29.4	85	32.2	90	23.9	75	Steady, wet coil
2	46.1	115	22.2	72	29.4	85	17.2	63	Steady, dry coil
3	40.6	105	22.8	73	29.4	85	17.2	63	Steady, dry coil
4/A	35	95	23.9	75	26.7	80	19.4	67	Steady, wet coil
5	29.4	85	17.2	63	23.9	75	13.9	57	Steady, dry coil
6	23.9	75	17.2	63	25	77	13.9	57	Steady, dry coil
B	27.8	82	18.3	65	26.7	80	19.4	67	Steady, wet coil
C	27.8	82	18.3	65	26.7	80	13.9	57	Steady, dry coil

3.2 Model Tuning

There was a systematic bias between the simulation and experimental results due to simplifications and imperfect information related to the EVI system components. To minimize the bias, 10 tuning multipliers were introduced to adjust mass flow rates, heat transfer coefficients and pressure drop on both air-side and refrigerant-side for the condenser and evaporator model as well as the cold-side and hot-side in the economizer model. The estimation of the multipliers was conducted by means of an iterative scheme to eliminate the discrepancy between the experimental results and the estimations of the suction and injection mass flow rates, the condenser, evaporator and economizer heat transfer rates, and the compressor power consumption. The optimization problem was solved with a bounded sequential least squares (SLSQ) method (Kraft, 1988), and the resulted tuning factors are listed in Table 10.

Table 10: Tuning multipliers for EVI system.

Compressor displacement scale factor	1.09
Condenser air-side convection heat transfer coefficient	0.75
Condenser refrigerant-side convection coefficient	0.75
Condenser refrigerant-side pressure drop correlation	0.95
Evaporator air-side convection heat transfer coefficient	0.75
Evaporator refrigerant-side convection coefficient	0.75
Evaporator refrigerant-side pressure drop correlation	1.2
Economizer cold-side convection coefficient	1.25
Economizer hot-side pressure drop correlation	0.95
Economizer cold-side pressure drop correlation	0.87

3.3 Model Validation

The validation was carried out with only the 8 test conditions stated in Table 9, which were experimentally investigated on a retrofitted ECU with EVI system with superheated injection ($T_{sh,inj}$ = 7°C). The comparisons of the refrigerant suction mass flow rate, the injection mass flow rate, the compressor discharge temperature and the power consumption as well as the system COP between the model simulations and the experimental results are illustrated in Figure 3. The percentage error between the predicted and experimental values is calculated by the mean absolute error (MAE) and the root mean square deviation (RMSD). Figure 3 shows that the tuned model captured the system and component performance within a reasonable margin of error. The minimum MAE and RMSD of 1.1% and 1.8% were estimated for the refrigerant suction mass flow rate, while the maximum MAE and RMSD of 5.7% and 5.6% were associated with the predictions of the compressor power consumption.

By using the charge model (Table 8) and the system tuning factors (Table 10), and by imposing the system charge inventory, the cycle was simulated at the conditions stated in Table 9 to assess the charge estimation as shown in Figure 4. Figure 4 compares the charge predictions for the cases without any correction, with one-point regression charge model, and with two-point model. It can be seen that the one-point charge model eliminates all the biases and predicts the charge inventory with MAE and RMSE less than approximately 0.2%, while the two-point charge model (Shen et al., 2009) perfectly estimates the system charge with no errors.

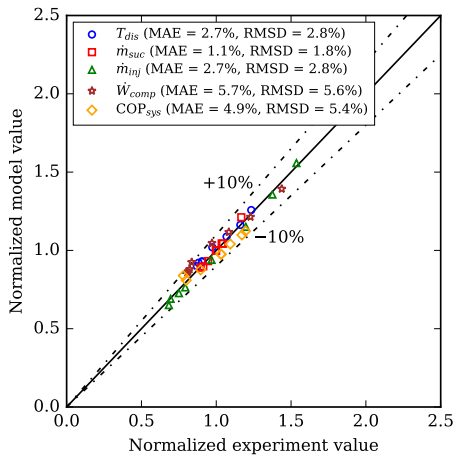

Figure 3: Comparison of estimated model performance parameters with experimental data for EVI system (normalized with average experimental value).

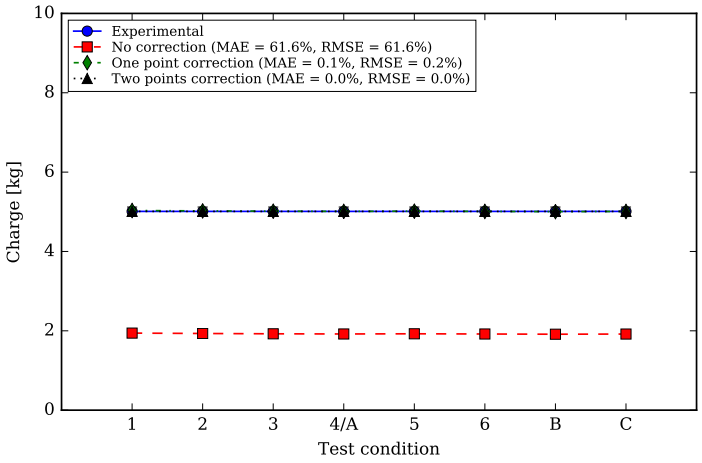

Figure 4: Comparison of charge prediction results with experimental data using one- and two-point regression charge model for EVI system at different testing conditions.

4. CONCLUSIONS

This paper aimed to develop a detailed model for an economized vapor injection (EVI) cycle to accurately estimate the amount of refrigerant charge inventory. This way, the system can efficiently operate at optimal condition with the optimal required charge. The EVI system model was tunned and validated with experimental data from a retrofitted Environmental Control Unit (ECU) tested at high ambient conditions in the Herrick Laboratories. The results yield the following conclusions:

- The mechanistic EVI system model predicted the performance parameters (*i.e.,* discharge temperature, suction and injection mass flow rates, compressor power, and system COP) with a reasonable margin of MAE less than approximately 5%.
- Charge imposed model with one- and two-point correction methods counted for the discrepancy in refrigerant charge estimation with MAE and RMSE less than approximately 0.2%.

ACKNOWLEDGEMENT

The authors would like to acknowledge the support from the Center for High Performance Buildings (CHPB) at the Ray W. Herrick Laboratories.

REFERENCES

Bell, I. H. (2015). Air conditioning and heat pump model (achp) source code version 1.5. [Online; accessed 10-Apr-2018].

Bell, I. H., Quoilin, S., Georges, E., Braun, J. E., Groll, E. A., Horton, W. T., and Lemort, V. (2015). A generalized moving-boundary algorithm to predict the heat transfer rate of counterflow heat exchangers for any phase configuration. *Applied Thermal Engineering*, 79:192–201.

Bell, I. H., Wronski, J., Quoilin, S., and Lemort, V. (2014). Pure and pseudo-pure fluid thermophysical property evaluation and the open-source thermophysical property library CoolProp version 6.1.0. *Industrial & Engineering Chemistry Research*, 53(6):2498–2508.

Bertsch, S. S. and Groll, E. A. (2008). Two-stage air-source heat pump for residential heating and cooling applications in northern U.S. climates. *International Journal of Refrigeration*, 31(7):1282–1292.

Braun, J. E. (1988). *Methodologies for the Design and Control of Central Cooling Plant*. PhD thesis, University of Wisconsin - Madison.

Brent, R. P. (1973). *Algorithms for minimization without derivatives*. Englewood Cliffs, NJ: Prentice-Hall.

Broyden, C. G. (1965). A class of methods for solving nonlinear simultaneous equations. *Mathematics of computation*, 19(92):577–593.

Chang, Y.-J., Hsu, K.-C., Lin, Y.-T., and Wang, C.-C. (2000). A generalized friction correlation for louver fin geometry. *International Journal of Heat and Mass Transfer*, 43(12):2237–2243.

Cho, I. Y., Seo, H. J., Kim, D., and Kim, Y. (2016). Performance comparison between R410A and R32 multi-heat pumps with a sub-cooler vapor injection in the heating and cooling modes. *Energy*, 112:179–187.

Churchill, S. W. (1977). Friction-factor equation spans all fluid-flow regimes. *Chemical engineering*, 84(24):91–92.

Claesson, J. (2004). *Thermal and Hydraulic Performance of Compact Brazed Plate Heat Exchangers Operating as Evaporators in Domestic Heat Pumps*. PhD thesis, KTH.

Cooper, M. G. (1984). Heat Flow Rates in Saturated Nucleate Pool Boiling-A Wide-Ranging Examination Using Reduced Properties. *Advances in Heat Transfer*, 16:157–239.

Gnielinski, V. (1976). New equations for heat and mass-transfer in turbulent pipe and channel flow. *International chemical engineering*, 16(2):359–368.

Harms, T. M. (2002). *Charge Inventory System Modeling and Validation for Unitary Air Conditioners*. PhD thesis, Purdue University.

Hong, K. T. and Webb, R. L. (1996). Calculation of fin efficiency for wet and dry fins. *HVAC&R Research*, 2(1):27–41.

Kim, M. H. and Bullard, C. W. (2002). Air-side thermal hydraulic performance of multi-louvered fin aluminum heat exchangers. *International Journal of Refrigeration*, 25(3):390–400.

Kim, S. M. and Mudawar, I. (2012). Universal approach to predicting two-phase frictional pressure drop for adiabatic and condensing mini/micro-channel flows. *International Journal of Heat and Mass Transfer*, 55(11-12):3246–3261.

Kim, S. M. and Mudawar, I. (2013). Universal approach to predicting heat transfer coefficient for condensing mini/micro-channel flow. *International Journal of Heat and Mass Transfer*, 56(1-2):238–250.

Kraft, D. (1988). A software package for sequential quadratic programming.

Lee, D., Seong, K. J., and Lee, J. (2015). Performance investigation of vapor and liquid injection on a refrigeration system operating at high compression ratio. *International Journal of Refrigeration*, 53:115–125.

Lee, H. S. (2010). *Thermal design: heat sinks, thermoelectrics, heat pipes, compact heat exchangers, and solar cells*. John Wiley & Sons.

Li, H. and Braun, J. E. (2008). A method for modeling adjustable Throat-Area expansion valves using manufacturers' rating data. *HVAC and R Research*, 14(4):581–595.

Lockhart, R. and Martinelli, R. (1949). Proposed correlation of data for isothermal two-phase, two-component flow in pipes. *Chemical Engineering Progress*, 45(1):39–48.

Longo, G. A. (2010). Heat transfer and pressure drop during HFC refrigerant saturated vapour condensation inside a brazed plate heat exchanger. *International Journal of Heat and Mass Transfer*, 53(5-6):1079–1087.

Longo, G. A. (2011). The effect of vapour super-heating on hydrocarbon refrigerant condensation inside a brazed plate heat exchanger. *Experimental Thermal and Fluid Science*, 35(6):978–985.

Longo, G. A., Gasparella, A., and Sartori, R. (2004). Experimental heat transfer coefficients during refrigerant vaporisation and condensation inside herringbone-type plate heat exchangers with enhanced surfaces. *International Journal of Heat and Mass Transfer*, 47(19-20):4125–4136.

Lumpkin, D. R., Bahman, A. M., and Groll, E. A. (2018). Two-phase injected and vapor-injected compression: Experimental results and mapping correlation for a R-407C scroll compressor. *International Journal of Refrigeration*, 86:449–462.

Martin, H. (2010). *VDI Heat Atlas*, chapter B6: Pressure Drop and and Heat Transfer in Plate Heat Exchangers. Springer Berlin Heidelberg, Berlin, Heidelberg, 2nd edition.

Moré, J., Garbow, B., and Hillstrom, K. (1980). User guide for MINPACK-1.
Python, S. F. (2016). Python language reference, version 2.7.13.
Schmidt, T. (1945). *La production calorifique des surfaces munies d'ailettes*.
Shah, M. M. (1976). A new correlation for heat transfer during boiling flow through pipes. *ASHRAE Transactions*, 82:66–86.
Shen, B., Braun, J. E., and Groll, E. A. (2009). Improved methodologies for simulating unitary air conditioners at off-design conditions. *International Journal of Refrigeration*, 32(7):1837–1849.
Standard, A. (2008). ANSI/AHRI Standard 210/240. *Performance rating of unitary A/C and air-source heat pump equipment*.
Sun, H., Hu, H., Wu, J., Ding, G., Li, G., Wu, C., Wang, X., and Lv, Z. (2018). Modèle de calcul théorique explicite pour les compresseurs à spirale à vitesse variable avec injection de vapeur. *International Journal of Refrigeration*, 88:402–412.
Tello-Oquendo, F. M., Navarro-Peris, E., and Gonzálvez-Maciá, J. (2017). New characterization methodology for vapor-injection scroll compressors. *International Journal of Refrigeration*, 74:528–539.
Tello-Oquendo, F. M., Navarro-Peris, E., Gonzálvez-Maciá, J., and Corberán, J. M. (2016). Performance of a scroll compressor with vapor-injection and two-stage reciprocating compressor operating under extreme conditions. *International Journal of Refrigeration*, 63:144–156.
Wang, B., Shi, W., Han, L., and Li, X. (2009). Optimization of refrigeration system with gas-injected scroll compressor. *International Journal of Refrigeration*, 32(7):1544–1554.
Wang, C.-C., Tsai, Y.-M., and Lu, D.-C. (1998). Comprehensive study of convex-louver and wavy fin-and-tube heat exchangers. *Journal of Thermophysics and Heat Transfer*, 12(3):423–430.
Zivi, S. M. (1964). Estimation of steady-state steam void-fraction by means of the principle of minimum entropy production. *Journal of Heat Transfer*, 86(2):247–251.

NOMENCLATURE

D	Diameter	(m)	**Superscripts**	
h	Enthalpy	(kJ/kg)	*	effective
m	Refrigerant charge	(kg)	**Subscripts**	
$\dot{m}$	Mass flow rate	(kg/s)	*a*	air
P	Pressure	(kPa)	*c*	cold
$\dot{Q}$	Heat rate	(kW)	*comp*	compressor
T	Temperature	(°C or K)	*cond*	condenser
V	Volume	(m^3)	*dis*	discharge
w	Area ratio	(–)	*down*	downstream
$\dot{W}$	Power	(kW)	*econ*	economizer
x	Quality	(–)	*evap*	evaporator
Acronyms			*h*	hot
COP	Coefficient Of Performance	(–)	*in*	inlet
ECU	Environmental Control Unit	(–)	*inj*	injection
EVI	Economized Vapor Injection	(–)	*int*	intermediate
EXV	Electronic Expansion Valve	(–)	*liq*	liquid
MAE	Mean Absolute Error	(%)	*out*	outlet
PHX	Plate Heat Exchanger	(–)	*pred*	predicted
RMSD	Root Mean Square Deviation	(%)	*r*	refrigerant
TXV	Thermostatic Expansion Valve	(–)	*ref*	reference
Greek symbols			*sh*	superheated
Δ	Residual	(units vary)	*suc*	suction
ρ	Density	(kg/m^3)	*sys*	system
ε	Effectiveness	(–)	*tot*	total
ζ	Solubility	(–)	*up*	upstream